

pubs.acs.org/estwater Article

Effects of Iron and Dissolved Organic Matter on Bioavailability of Arsenite under Anaerobic Conditions

Hyun Yoon, Benjamin Stenzler, Lena Abu-Ali, Maria P. Asta, Alexandre J. Poulain, and Matthew C. Reid*



Cite This: ACS EST Water 2023, 3, 3676-3686



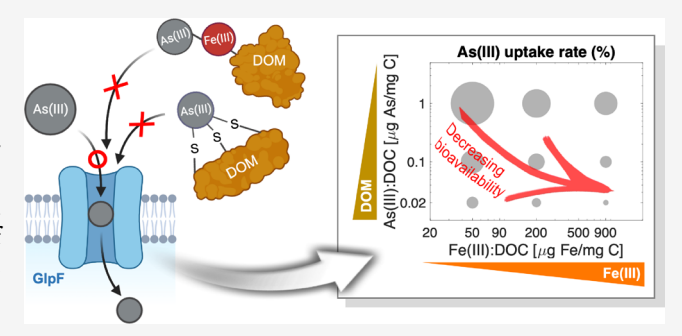
ACCESS

III Metrics & More

Article Recommendations

s Supporting Information

ABSTRACT: Understanding the effects of water chemistry on the availability of arsenic (As) to biota is important for predicting the environmental fate of As. The "dissolved" fraction of As (<0.22 μ m) is often used as a proxy for bioavailable As. However, As speciation is also influenced by binding to dissolved organic matter (DOM) and colloidal iron (Fe) (oxy)hydroxides, which can impact bioavailability. Here, we use a recently developed *Escherichia coli* anaerobic biosensor to elucidate the effects of DOM and Fe on arsenite (As(III)) bioavailability under anaerobic conditions, where As can be highly mobile. Microbial As(III) uptake decreased with greater DOM and Fe(III) concentrations, while Fe(II) had no effect. Higher organic sulfur content in DOM



was associated with decreased biouptake at low As(III)/C ratios, and X-ray absorption spectroscopy indicated that this was due to binding of As(III) to sulfur ligands like thiols. The 0.1-0.5 kDa size fraction of As was most closely related to the bioavailable As fraction. Because the aquaporin channels mediating As(III) uptake into both microbes and rice plants are structurally similar, our results may also have relevance for understanding of how biogeochemical conditions in rice paddies regulate the plant availability of arsenic.

KEYWORDS: arsenic, arsenite, microbial uptake, bioavailability, biosensor, iron, dissolved organic matter, colloids, thiols, EXAFS

■ INTRODUCTION

Arsenic (As) is a nonthreshold carcinogen that is ubiquitous in the environment and is an important contaminant in water and food. There is particularly active research interest in biogeochemical As dynamics in rice paddy soils $^{1-4}$ due to concerns around human exposure to As through consumption of rice, a dietary staple for half of the global population. Arsenic mobility in subsurface environments is greatly enhanced under anaerobic conditions due to the reductive dissolution of As-bearing Fe(III) (oxy)hydroxide minerals and by the reduction of arsenate (As(V)) to arsenite (As(III)). $^{5-8}$ In waters that are rich in dissolved organic matter (DOM) and/or iron (Fe), mobilized As is often associated with colloidal particles. $^{9-11}$ This occurs via direct binding with organic ligands in DOM molecules, 12 ternary complexation via Fe-bridging, $^{13-15}$ and association with colloidal Fe(III) (oxy)hydroxides. 9,10,16

Fe(III)-rich colloids are produced by the oxidation of Fe(II) at oxic-anoxic interfaces, and DOM partially stabilizes this colloidal Fe(III) by inhibiting the aggregation of Fe(III) (oxy)hydroxides. ^{17,18} In rice paddy and other DOM-rich wetland soils, radial oxygen loss from aerenchymal roots of wetland plants creates extensive oxic-anoxic interfaces in the rhizosphere where these redox reactions of Fe can occur.

These reactions form Fe(III) plaques on root surfaces, which impact As mobility and bioavailability, ^{19–21} and may also lead to production of colloidal Fe(III) in the rhizosphere. Water level fluctuations in wetlands, including deliberate alternate wetting and drying (AWD) of rice paddy soils to decrease plant availability of As, ^{22,23} also introduce oxic-anoxic interfaces that can promote formation of DOM-Fe colloidal phases. ²⁴ Ultrafiltration and diffusive gradients in thin-film investigations have shown that complexed and/or colloidal As can be an important fraction of soil solution As. ²⁵

Direct binding of As(III) to DOM can also be significant without complexed or colloidal Fe and is a function of As(III)/C ratios and DOM properties. 12,26,27 The organic sulfur (S $_{\rm Org}$) content of DOM has been linked to greater As(III) complexation, 26,28 and this is thought to be due to the role of thiol (sulfhydryl) ligands as As(III) binding sites. $^{29-31}$ Elucidating the effects of DOM functional groups and other

Received: August 2, 2023 Revised: October 10, 2023 Accepted: October 11, 2023 Published: October 23, 2023





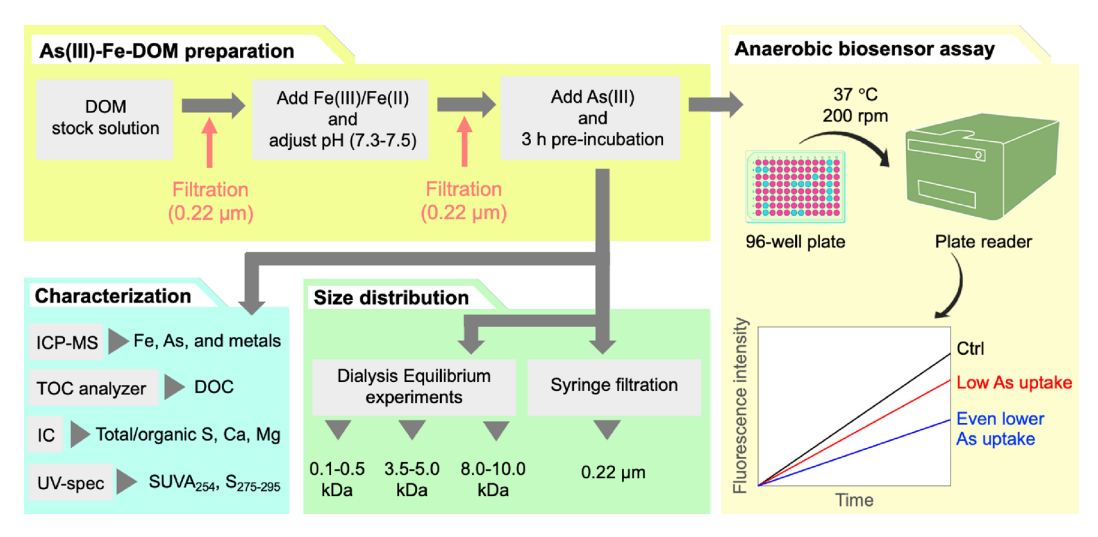


Figure 1. Workflow of procedures for producing Fe-DOM solutions reacted with As(III) for use in anaerobic biosensor and dialysis experiments.

properties on the environmental fate of As is a topic of active research. 32-34 Relevant forms of DOM in rice paddy soils include humic materials from the decomposition of plant biomass as well as DOM derived from algae, which can grow in the standing surface water of rice paddies 35 and can contribute to As association with colloids. Despite the well-recognized importance of As-Fe-DOM interactions in the environment, there have been few studies that investigate the bioavailability of As(III) in Fe- and DOM-rich waters.

The objective of this research was to evaluate the bioavailability of As(III) in waters containing DOM with both ferrous and ferric Fe, where significant portions of As will be in colloidal size fractions. This research interrogates the assumption that As concentrations in filtered pore water are good predictors of bioavailability,³⁷ with a focus on waters with high concentrations of S_{Org}-rich DOM and/or Fe-DOM colloids. To obtain direct and high-throughput measurements of bioavailability in anaerobic conditions relevant for flooded paddies or groundwater, we use a recently developed anaerobic biosensor method.³⁸ Arsenic biosensors have traditionally been limited to aerobic conditions due to the requirement for oxygen for the maturation of conventional fluorophores. Here, the anaerobic biosensor construct enables measurements with reduced species including As(III) and Fe(II), as well as reduced moieties in DOM like thiols.³⁰ We hypothesize that (i) DOM and Fe control cellular As(III) uptake due to the role of DOM-stabilized Fe colloids in binding As(III), (ii) As(III) complexation with thiol ligands will lead to greater inhibition of As(III) uptake in S_{Org}-rich DOM, and (iii) unbound or "free" As in the 0.1-0.5 kDa fraction is the best predictor of As bioavailability, since this range of molecular size is the closest to the pore size of the aquaglyceroporin protein GlpF that mediates As(III) transport across microbial cell membranes. 39,40

MATERIALS AND METHODS

Dissolved Organic Matter Samples and Preparation of Fe-DOM Solutions. DOM samples were prepared from Aldrich humic acid (AHA; Sigma-Aldrich, St. Louis, MO), which has been used in a number of previous studies on metal(loid)-DOM complexation, 10,17,41,42 as well as the International Humic Substances Society (IHSS) products Upper Mississippi River natural organic matter (MNOM) and

Suwannee River humic acid (SRHA). Anoxic solutions were prepared in autoclaved degassed Milli-Q water in a Coy anaerobic chamber (98% N₂, 2.0% H₂). After vacuum filtration through a 0.22 μ m membrane filter (Corning, Corning, NY), solutions were diluted to a range of target dissolved organic carbon (DOC) concentrations (40, 400, and 2000 mg C/L for AHA and 20, 100, and 400 mg C/L for MNOM and SRHA). As part of a separate project, we sampled algal biomass floating in a rice paddy in Lonoke, Arkansas (34°35′32.478″ to 91°42′53.892″). Algal biomass was sonicated with Milli-Q water for 2 h and vacuum-filtered (0.22 μ m). The filtered algal DOM extract was immediately purged with nitrogen gas and stored in rubber stopper-sealed vials at 4 °C until use.

The workflow for Fe-DOM solution preparation and the biosensor assay is summarized in Figure 1. Iron was added to the DOM solutions as FeCl₃·6H₂O (Fisher Scientific, Waltham, MA) or FeCl₂ (Sigma-Aldrich, St. Louis, MO), modified from the method described in Liu et al. 10 Iron salts were slowly dissolved and mixed with DOM inside the anaerobic chamber, while pH was maintained between 7.3 and 7.5 using NaOH to achieve Fe(III)/C ratios between 0 and 900 μ g Fe(III)/mg C. Fe(II) was added to AHA solutions under anaerobic conditions at the ratios of 50, 200, and 900 μ g Fe/mg C, with the pH maintained in the range of 7.3-7.5. Higher Fe/C ratios will lead to higher concentrations of DOMstabilized Fe colloids, 17 allowing us to test hypotheses on the role of DOM-stabilized Fe colloids in controlling As(III) bioavailability. Fe-DOM solutions were then filtered through a 0.22 µm membrane before further analyses. Fe/C ratios were confirmed using measurements of DOC (NPOC method) and Fe (ICP-MS) in solutions used in biosensor assays (Table 1).

A matrix of As-Fe-DOM solutions was prepared to systematically assess the effects of different As(III)/C ratios (Fe and As(III) concentrations fixed) and Fe/C ratios (C and As(III) concentrations fixed) on microbial As(III) uptake. As(III)/C ratios ranged from 0.02 to 2 μ g As/mg C (Table 1) and were selected based on observations of relevant As(III)/C ratios in rice paddy soil pore waters. As(III) concentrations were held constant at 18.75 μ g/L As(III) in all experiments to compare biosensor results across different experimental conditions. ICP-MS analysis showed that the intrinsic As concentration in the algal DOM extracts was relatively high (>35.63 μ g/L), so samples were diluted until As_{Tot} < 1.88 μ g/

Table 1. Summary of DOM Characterization Used in This Study^f

			$As(III)/C$ (μ	As(III)/C (µg As/mg C)	Fe(.	Fe(III)/C (µg Fe/mg C)					
DOM type	source	DOC (mg C/L)	intrinsic	after As amendment	intrinsic	after Fe amendment	Fe(II)/C ($\mu g Fe/mg C$)	S _{Tot} /C (mg S/mg C)	$S_{Org}/C \text{ (mg S/} SUVA_{254}^{b}$ $mg \text{ C)} \text{ (L } mg^{-1}\text{ m}^{-1})$	$\frac{\text{SUVA}_{254}}{(\text{L mg}^{-1} \text{m}^{-1})}$	$S_{275-295} ({ m nm}^{-1})$
AHA	Sigma-Aldrich	$^{\sim}20, ^{\sim}200, \text{ and } ^{\sim}1000^d$	0.000	$\sim 0.02, \sim 0.1, \text{ and } \sim 1$	0.79	$\sim 20, \sim 50, \sim 90, \sim 200, \sim 500, \sim 900^d$	0.003	$0.017 (0.011)^a$	0.015	3.05	0.003
MINOM	SSHI	$^{\sim}10, ^{\sim}50, \text{ and}$ $^{\sim}200^{d}$	0.000	~ 0.1 , ~ 0.4 , and $\sim 2^4$	0.89	$\sim \! 50, \sim \! 200, \sim \! 900^d$	0.543	$0.052 (0.052)^a$	0.019	2.07	0.004
SRHA	SSHI	$\sim 10, \sim 50, $ and $\sim 200^{d}$	0.000	$\sim 0.1, \sim 0.4, \text{ and}$ $\sim 2^d$	1.25	$\sim 50, \sim 200, \sim 900^d$	0.003	$0.011 (0.011)^a$	0.009	3.35	0.003
Algae 1	rice paddy algae extract	18.8	$0.029 (0.050)^e$	1.025	16.45	16.45	0.686	0.052	0.009	0.13	0.010
Algae 2	rice paddy algae extract	28.2	$0.028 (0.033)^e$	0.694	11.55	11.55	0.727	0.048	9000	0.13	0.006
Algae 3	rice paddy algae extract	77.8	$0 (0.011)^e$	0.241	96.6	96.6	3.110	0.026	0.003	0.30	0.012
Algae 4	rice paddy algae extract	8.66	0 (0.009)	0.188	12.56	12.56	2.462	0.025	0.002	0.13	0.023

*Numbers in parentheses are S_{Tot}/C reported by the manufacturer (Sigma-Aldrich and IHSS). *SUVA₂₅₄ was used to determine aromaticity using the equation SUVA₂₅₄ = UV₂₅₄/C.** *Spectral slope (S255-295) was used to determine mean molecular weight, as described by Helms et al. 57 dNumbers with tilde are target values. Measured values were used for the bubble plot and three-dimensional scatter plot. "Numbers in parentheses are total As/C, which includes methylated As and arsenate, measured with HPLC-ICP-MS. Information on trace metal contents is available in Table SI. L, and then As(III) from the sodium arsenite stock solution was added to reach a concentration of 18.75 μ g/L.

Anaerobic Biosensor Assay for Cellular As(III) Uptake. A recently developed whole-cell anaerobic arsenic biosensor³ was used to quantify As uptake rates under anoxic conditions. The biosensor is an Escherichia coli NEB5 α containing a plasmid with the fusion of the arsenic-sensing arsR promoter and reporter gene encoding a Pseudomonas putida flavin-based fluorescent protein (PpFbFp) that does not require O2 for signal production (Figure S1a). Supporting experiments were performed using the biosensor with constitutive expression of PpFbFp to show that changes in fluorescence intensity were due to changes in cellular As uptake only and not to cellular responses to other variations in matrix constituents. See the Supporting Information for more details on the constitutive biosensor experiments. Biosensor cells and experimental media were all maintained under strict anoxic conditions throughout all experimental procedures.

For each biosensor assay, *E. coli* biosensor cells were plated onto an LB plate supplemented with 120 μ g/mL ampicillin and incubated overnight at 37 °C. Independent colonies were then inoculated into balch tubes containing 5 mL of growth media in the anaerobic chamber. Balch tubes were sealed with butyl rubber stoppers and incubated on an orbital shaker at 37 °C and 200 rpm. Cell growth was monitored using an optical density at 600 nm (OD₆₀₀). Once OD₆₀₀ reached ~0.6, 200 μ L of the washed biosensor cells was added to the exposure media. The exposure media contained 18.75 μ g/L As(III) that had been preincubated with Fe-DOM solutions for 3 h in the anaerobic chamber. The biosensor was grown with pyruvate as the electron donor and fumarate as the electron acceptor. Additional details about the growth and exposure media are provided in the Supporting Information.

Biosensor assays in biological triplicates were prepared in 96-well plates, and As(III) uptake was determined through fluorescence intensity measurements at 2.5 min intervals for 10 h at 37 °C using a Synergy HTX plate reader inside the anaerobic chamber. Fluorescence of PpFbFp (excitation wavelength, 440 nm; emission wavelength, 500 nm) and OD₆₀₀ were measured. We recently developed a mathematical model to describe cellular As(III) uptake rates based on a time series of biosensor fluorescence⁴³ (see the Supporting Information for further details on model development). This model showed that the net As(III) uptake rate at time t, $\mu(t)$ (mg As mg biomass⁻¹ h⁻¹), can be described as

$$\mu(t) \propto \sqrt{\frac{1}{N(t)} \frac{\mathrm{d}F_{\mathrm{RFU}}}{\mathrm{d}t}} = \Psi(t)$$
 (1)

 $F_{\rm RFU}$ is the measured biosensor fluorescence intensity (RFU). N(t) is the biomass at time t (mg biomass mL⁻¹), converted from measured OD₆₀₀ through a calibration curve obtained through serial dilution (Figure S2).⁴⁴ The lumped parameter $\Psi(t)$ ($\sqrt{\rm RFU}(\rm mg\,biomass/mL)^{-1}h^{-1}$) describes the slope of the biomass-normalized fluorescence with respect to time and will be used hereafter to describe As(III) uptake rates as the measure of As(III) bioavailability.

Biosensor cells in the same Fe-DOM matrix without As(III) were run in parallel in biological triplicate for subtraction of background fluorescence. A reference uptake rate ($\Psi_{\rm ref}(t)$) was determined for each experimental condition using biosensor cells in the presence of 18.75 μ g/L As(III) without Fe or DOM. The reference uptake rates, $\Psi_{\rm ref}(t)$, were then used to

determine a relative As(III) uptake rate in the presence of the Fe-DOM matrix:

relative As(III)uptake rate(%) =
$$\frac{\Psi(t)}{\Psi_{Ref}(t)} \times 100$$
 (2)

Inhibition of As(III) uptake in the presence of Fe-DOM matrices was then quantified as

As(III)uptake inhibition(%)

$$= 100 - \text{relative As(III)} \text{uptake rate}$$
 (3)

Arsenic speciation analysis via HPLC-ICP-MS was performed with filtered As-Fe-DOM samples after 20 h in biosensor assays to assess the stability of As(III).

Size Fractionation of As(III) in Fe(III)-AHA Matrices. Dialysis equilibrium experiments were performed under anaerobic conditions to quantify size fractionation of As in the presence of Fe(III)-DOM matrices. 12,26 As(III)-Fe(III)-DOM solutions were prepared using the approach described above, with the exception that 37.5 μ g/L instead of 18.75 μ g/L As(III) was used because As(III) concentrations in the dialysate can be low and a higher initial concentration facilitated mass balance calculations using dialysate concentrations. Fe(III)/C ratios of 0, 50, 200, and 900 μ g of Fe/mg of C (fixed DOC with varying Fe(III)) were prepared. Solutions were transferred into triplicate 10 mL Float-a-Lyzer dialysis membranes (Spectra-Por) with three different pore sizes (0.1– 0.5, 3.5-5.0, and 8.0-10.0 kDa). Before the experiments, dialysis membranes were soaked in 20% ethanol for ~48 h and thoroughly rinsed with Milli-Q water to prevent carbon leaching from membranes during the experiment.

As(III)-Fe(III)-DOM solutions were dialyzed in 300 mL high-density polyethylene (HDPE) containers filled with a bulk solution of 0.1 M KCl, 5 mM MOPS buffer, and 0.15 mM sodium azide at pH 7 in an anaerobic chamber at room temperature. Note that these experiments were separate from biosensor experiments; therefore, at no point did biosensor cells come into contact with sodium azide. After 96 h of incubation, 10 mL aliquots from inside the membrane and from the bulk solution ($As_{in,96h}$ and $As_{out,96h}$, respectively) were collected to determine the ratio of As(III) retained within membranes of different pore sizes:

$$= \frac{(As_{\text{in},96\text{h}} - As_{\text{out},96\text{h}})V_{96\text{h}}}{As_{\text{in},0\text{h}}V_{0\text{h}}} \times 100\%$$
(4)

where $As_{\text{in,0h}}$ is the initial As concentration. $V_{96\text{h}}$ and $V_{0\text{h}}$ are the volumes inside the membranes (mL) at 96 and 0 h, respectively, which could experience small changes due to osmotic effects. Another portion was filtered through a 0.22 μ m membrane filter to determine the fraction of As(III) in size fractions >0.22 μ m. The As(III) retention ratio indicates the fraction of As in the sample with a size greater than a given pore size.

Pore sizes of membranes used in dialysis experiments were compared to the pore radii of the aquaporin channels GlpF and Lsi1 that mediate As(III) uptake into microbial and plant cells, respectively, to link As(III) size fractionation to transport through membrane channels. Structural models of GlpF and Lsi1 transporters were computed from protein sequences (Protein Data Bank accession: 1LDA⁴⁵ and 7CJS,³⁹ respectively) using Mole 2.5⁴⁶ and UCSF Chimera.⁴⁷

X-ray Absorption Spectroscopy. X-ray absorption spectroscopy (XAS) was performed to determine the complexation mechanisms between As(III) and DOM, with a focus on the role of S_{Org} ligands in binding As(III). A 25 μ g/L As(III) and 3.3 g C/L solution of AHA was mixed under anaerobic conditions for 24 h and then dialyzed with a 0.1-0.5 kDa membrane. This low As(III)/DOM ratio was used to avoid saturating the S_{Org} ligands. The solution remaining inside the dialysis tubing was then freeze-dried and stored in a N2-flushed and heat-sealed mylar bag until synchrotron analysis. Glutathione-bound As (As(GSH)₃) was synthesized⁴⁸ inside the anaerobic chamber as a reference for As coordinated with thiol ligands and collected on a filter, and an As(III) reference was prepared by wetting a kimwipe with a sodium arsenite solution and then drying the kimwipe.⁴⁹ The freeze-dried sample and references were enclosed in Kapton tape, and the EXAFS spectra were collected at beamline 6-BM at NSLS-II. The arsenic K-edge k^3 -weighted EXAFS spectra were analyzed by background subtraction, and the parameters were refined in nonlinear least-squares fits using the shell-by-shell method over a k range of 2 to up to 12 Å⁻¹ (depending on data quality) with the program EXAFSPAK. E_0 was set at 11885 eV. Theoretical single scattering reference functions calculated by the program FEFF⁵¹ using atomic clusters from crystalline reference As compounds were calculated with the program ATOMS.⁵²

Analytical Methods. Metal(loid) concentrations in Fe-DOM matrices were measured by ICP-MS (Agilent 7800; As, Fe, Mn, Al, Cu, and Zn) or cation-exchange ion chromatography (Dionex ICS-2100; Ca and Mg). Arsenic speciation in Fe-DOM matrices was monitored using HPLC-ICP-MS (Agilent Infinity 1260 HPLC hyphenated to Agilent 7800 ICP-MS), with an eluent of 6.66 mM ammonium phosphate and 6.66 mM ammonium nitrate, pH adjusted to 6.2.53 The ferrozine method with hydroxylamine⁵⁴ was used for determination of Fe(II)/Fe(III) ratios. DOC was measured using a Shimadzu TOC-L analyzer (NPOC method). Inorganic sulfur (S) species (sulfate, sulfite, and thiosulfate) in DOM samples were measured using anion-exchange chromatography, and sulfide was measured by the cline method.⁵⁵ The organic S (S_{Org}) content of DOM was determined by oxidizing S_{Org} to sulfate (SO_4^{2-}) via overnight incubation with 30% H_2O_2 and 0.1 M HCl.⁵⁶ The S_{Org} concentration was determined as the difference in the SO₄ concentrations before and after H₂O₂ oxidation (sulfide, sulfite, and thiosulfate were below the limit of detection in all samples). The DOM optical properties spectral slope $(S_{275-295})$ and SUVA₂₅₄ were measured using a Shimadzu UV-2600i spectrophotometer and were used as proxies for mean molecular weight⁵⁷ and aromaticity,⁵⁸ respectively.

Statistical Methods. A multiple linear regression model was fit to As(III) uptake rates for AHA-Fe(III) matrices as a function of log-transformed As(III)/C and Fe(III)/C ratios using the fit command in R.59 The model trained on the AHA data set was then used to predict As(III) uptake rates determined for other DOM samples. Goodness-of-fit metrics (mean absolute error (MAE) and root mean squared error (RMSE)) were determined and used to assess model skill in predicting As(III) uptake rates for diverse DOM samples as a function of As(III)/C and Fe(III)/C.

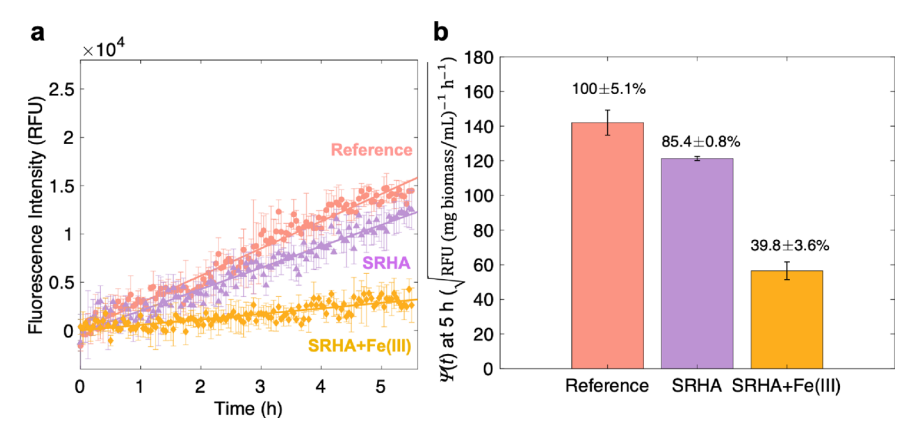


Figure 2. (a) Representative fluorescence data from the anaerobic biosensor assay with 18.75 μ g/L As(III) only (reference), 18.75 μ g/L As(III) + SRHA (0.4 μ g As/mg C; SRHA), and 18.75 μ g/L As(III) + SRHA + Fe(III) (0.4 μ g As/mg C and 900 μ g Fe/mg C). Symbols are average values, and error bars show the standard deviation of n = 3 biological triplicates. Linear regression lines were fit to fluorescence data, and the slopes were used for As(III) uptake rate quantification. (b) Bar plots of Ψ(t) at 5 h calculated using eq 1. Numbers above each bar show the relative As(III) uptake rate under each condition.

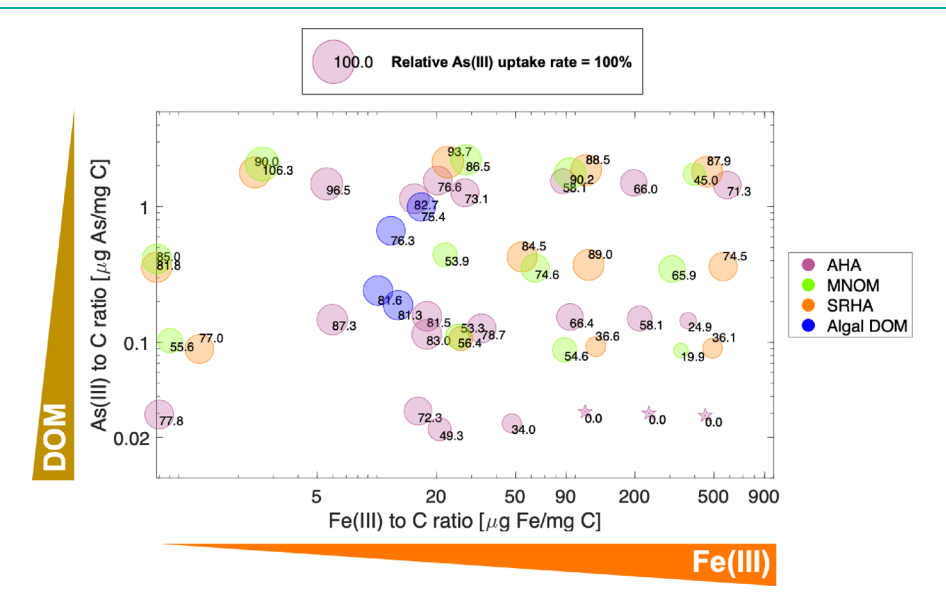


Figure 3. Relative As(III) uptake rates for different types of DOM at different As(III)-to-C and Fe(III)-to-C ratios. The size of the bubble corresponds to the relative As(III) uptake rate compared with the reference condition without DOM or Fe(III), and colors represent different types of DOM. The number next to each bubble is the relative uptake rate. As(III) was fixed at 18.75 μ g/L for all experiments. Along the *y*-axis, As(III) was fixed, and DOC was varied. Along the *x*-axis, DOC and As(III) were fixed, and Fe(III) was varied. Stars represent conditions where $\Psi(t)$ was zero and uptake was completely inhibited.

RESULTS

DOM Characterization. DOM samples examined in this study had diverse properties (Table 1). AHA, SRHA, and MNOM had greater aromaticity than the algal DOM extracts, while the spectral slope analysis showed that algal DOM also had a lower molecular weight. These results are consistent with expectations that the algal DOM extracts consisted of primarily smaller, nonaromatic cellular products compared to the other DOM products. MNOM had the highest S_{Org}/C ratio, in agreement with elemental compositions provided by IHSS. The algal DOM extracts had intrinsic concentrations of Fe(II) and Fe(III) that were higher than those of the IHSS products. Concentrations of other metals in the DOM samples are provided in Table S1.

Effects of Fe-DOM Matrices on As(III) Uptake. Arsenic was found to be stable as As(III) over 20 h of incubation with DOM or Fe(III)-DOM, with no evidence of As oxidation by

Fe(III) (Figure S3). Representative biosensor fluorescence data (Figure 2) show a decrease in dF_{RFU}/dt with an increase in DOM and Fe(III), indicating a decrease in cellular uptake rates. The uptake rate parameter $\Psi(t)$ decreased by 14.6(\pm 4.4)% in the presence of SRHA at a 0.4 μ g As/mg C ratio relative to the reference uptake rate in the absence of DOM, $\Psi_{ref}(t)$. Addition of 900 μ g of Fe(III)/mg of C (orange) led to a larger decrease of roughly $60.2(\pm 4.1)$ % relative to $\Psi_{ref}(t)$. Either similar or increased cell density (N(t)) was observed for all conditions relative to the reference biosensor assay without Fe or DOM (Figures S4 and S5), indicating that none of the experimental conditions had significant toxic effects on the biosensor cells. This finding is supported by results from constitutive biosensor experiments (Figure S6).

Relative As(III) uptake rates were determined for the full matrix of experimental conditions and mapped as a function of

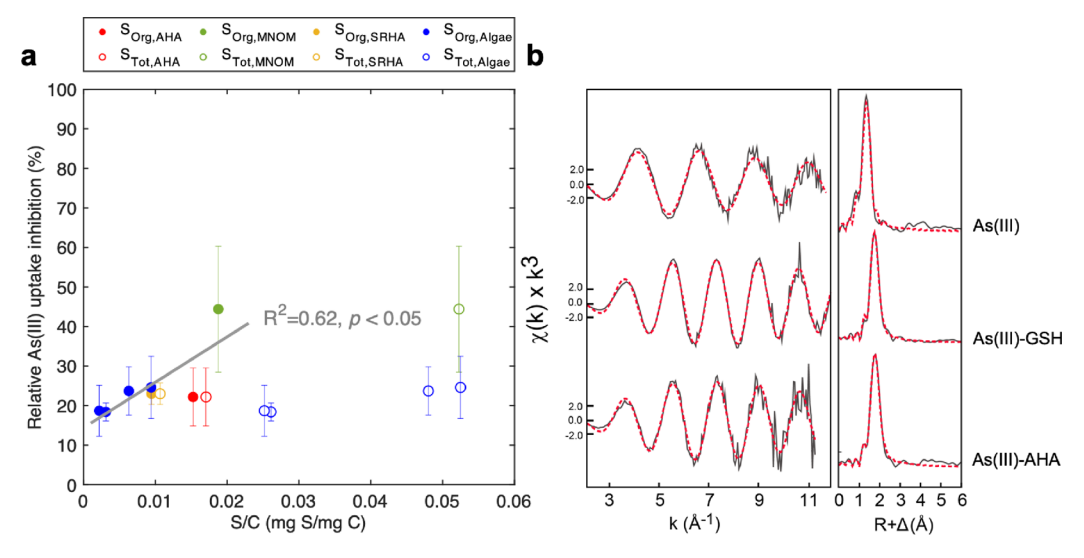


Figure 4. Correlation between S_{Org}/C (filled circles) or S_{Tot}/C (empty circles) ratios in different DOM samples and relative As(III) uptake inhibition. DOM samples with the lowest Fe/C (<50 μ g Fe/mg C) and lowest As/C ratios (<0.1 μ g As/mg C) were plotted along with the four algal DOM samples. The solid line is a linear regression for S_{Org}/C ($R^2 = 0.62$, p < 0.05). The regression line for S_{Tot}/C is not shown due to the lack of a significant correlation for S_{Tot}/C (p > 0.05) (b) EXAFS spectra (black line) and shell fitting (red dashed line) for As(III) and As(III)-GSH references and for a sample of As(III) that reacted with AHA (As(III)-AHA).

As(III)/C and Fe/C ratios (Figure 3; alternative visualizations are available in Figures S7 and S8). For each type of DOM, As(III) uptake rates decreased with higher concentrations of C (moving from top to bottom in Figure 3) and Fe(III) (moving from left to right in Figure 3). With AHA, $\Psi(t)$ was zero at the highest DOC and Fe(III) concentrations (As(III)/C ratio of 0.02 μ g/mg and Fe(III)/C ratios >50 μ g Fe/mg C), indicating that As(III) uptake was completely inhibited (star symbols in Figure 3).

A comparison across different types of DOM showed that the As(III) uptake rates generally followed the same patterns. In most cases, measurements with different types of DOM at similar As(III)/C and Fe(III)/C ratios showed comparable As(III) uptake rates ($\pm 15\%$), as can be seen by comparing overlapping or adjacent bubbles with different colors in Figure 3. One exception is MNOM, which tends to have lower As(III) uptake rates at similar As(III)/C and Fe(III)/C ratios to those of other DOM samples. Potential reasons for this are explained in the next section. A multivariate regression model adequately described variation in As(III) uptake in the presence of AHA as a function of log-transformed As(III)/C and Fe(III)/C ratios ($R^2 = 0.73$) (Figure S8a and Table S2). This model trained on the AHA data set provided good prediction of As(III) uptake rates with other DOM samples (RMSE, 3.5%) (Table S2), further showing that As(III) uptake rates were largely determined by As(III)/C and Fe(III)/C ratios, with variations in intrinsic DOM properties exerting a smaller control on uptake rates.

The anaerobic biosensor assay also enabled the assessment of the effects of Fe(II) on As(III) uptake. Fe(II)-AHA solutions were prepared by using the same procedures as those for Fe(III)-AHA, spanning the same range of Fe/C ratios tested for Fe(III). Fe(II) showed negligible effects on As(III) uptake at all Fe(II)/C (Figure S9).

Effects of S_{Org} and Other DOM Properties on As(III) Uptake. S_{Org} ligands like thiols have been suggested as strong binding sites for As(III) in DOM, ^{26,28,30} and we hypothesized that differences in the S_{Org}/C ratio of DOM samples may be a good predictor of As(III) uptake inhibition by DOM. While

the proposed mechanism involves thiols, we use S_{Org} as a proxy for thiols since direct measurement of thiol concentrations is difficult in samples containing fluorescent DOM. Because densities of S functional groups in DOM are low, 60 we first considered data from experiments at low As(III)/C ratios, along with experiments with the environmental algal DOM extracts where only one As(III)/C ratio was used. Consistent with our hypothesis, the S_{Org}/C ratio was a good predictor of As(III) uptake inhibition in this set of conditions ($R^2 = 0.62$; p< 0.05; Figure 4a). The S_{Org}/C ratio of MNOM was 2.1 times higher than SRHA, closely matching the differences in As(III) uptake rate inhibition (44.4 \pm 16.0% for MNOM vs 23.0 \pm 2.7% for SRHA). The higher S_{Org} content of MNOM may explain why As(III) uptake rates for MNOM tended to be lower than those for other DOM samples at similar As(III)/C and Fe(III)/C ratios (Figure 3). This relationship between S_{Org}/C and As(III) uptake inhibition did not hold at higher As(III)/C (Figure S10), suggesting that once DOM thiols were saturated, the S_{Org} content did not affect bioavailability. There was also no relationship between S_{Org}/C and uptake in experiments with added Fe(III) (Figure S10).

EXAFS analysis of As(III) reacted with AHA at a low As(III)/C ratio, and no added Fe showed that As was coordinated with S atoms (Figure 4b), providing an explanation for why the S_{Org} content of DOM is related to variations in As uptake rates. The As(III)-AHA EXAFS spectra were found to be similar to the As(GSH)₃ standard, with As(III) coordinated to 3 S atoms and an interatomic distance of 2.26 Å (Figure 4b and Table S3). This shows that in the absence of complexed Fe(III), As(III) was directly bound to S ligands in the AHA matrix. There was no relationship between the aromaticity or mean molecular weight of DOM samples and As(III) uptake (Figure S11).

Size Distribution of As(III) Reacted with Fe(III)-AHA. Retention ratios of As(III) bound to AHA or complexed/colloidal Fe(III)-AHA were determined using eq 4 and can be interpreted as the % of As(III) associated with a complex or colloid larger than a given pore size. Only $4.5 \pm 0.9\%$ of As(III) was bound to humic molecules in AHA with a size

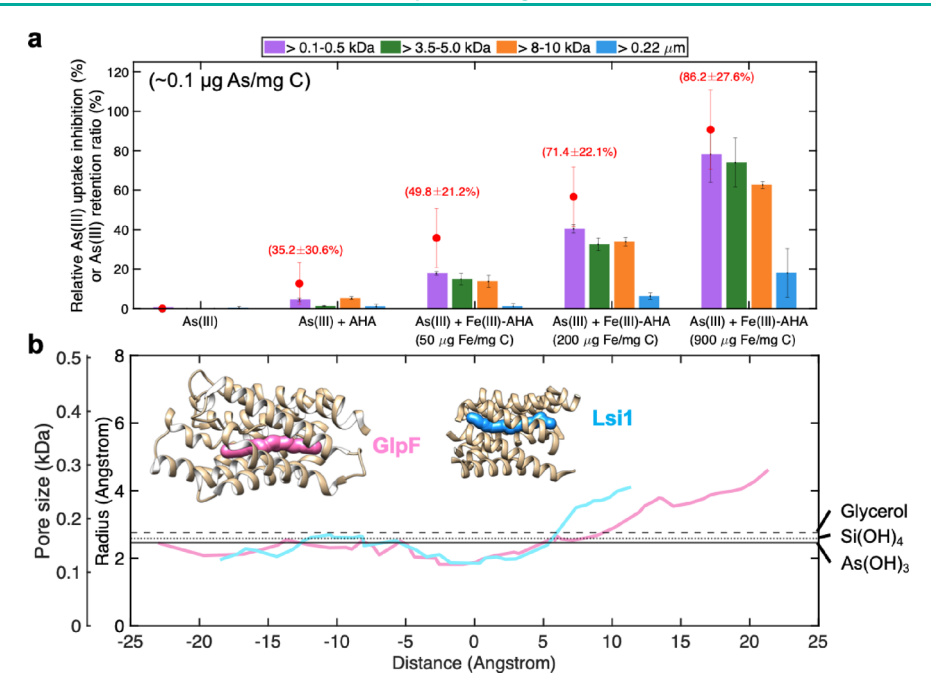


Figure 5. (a) Dialysis data on the size fractionation of As in the presence of AHA and Fe(III)-AHA matrices over a range of Fe(III)/C (bars) and biosensor data on As(III) uptake inhibition (red circles). Different colored bars represent different size fractions. Numbers in parentheses denote the fraction of total uptake inhibition (red circle) that can be explained by the fraction of As > 0.1-0.5 kDa (purple bar). (b) Pore radii of GlpF (pink) and Lsi1 transporter (light blue) along the membrane transport channel in units of kDa and angstroms. The sizes of glycerol, orthosilicate (Si(OH)₄), and As(OH)₃ based on van der Waals volume are shown in lines (black dashed, dotted, and solid line, respectively) and are included since these substrates are taken up through GlpF channels in bacteria (glycerol, arsenite) and Lsi1 channels in rice plants (orthosilicate, arsenite).

greater than 0.1–0.5 kDa at a ratio of 0.1 μ g As/mg C ratio with no added Fe(III), with the balance of the As(III) present as unbound or "free" As(III). The size fraction of As(III) > 0.1-0.5 kDa increased as Fe(III)/C ratios increased, reaching up to $78.1 \pm 14.0\%$ at the highest Fe(III)/C. As expected, the smallest pore size of 0.1-0.5 kDa had the highest As(III) retention ratios at all Fe(III)/C ratios. However, the differences in the As(III) binding ratio across different pore sizes were negligible for all Fe(III)/C ratios, except for the 900 μ g Fe/mg C ratio and for size fractions >0.22 μ m. This indicates that most of the bound As(III) was in the colloidal size fraction larger than 8.0-10.0 kDa but smaller than 0.22 um. The fact that a small fraction of the As(III) was determined to be in the size fraction >0.22 μ m at the end of dialysis experiments suggests that there was aggregation of colloids during the dialysis experiments, since Fe(III)-AHA solutions were filtered through 0.22 μ m filters before the start of dialysis experiments.

As(III) in the size fraction >0.1-0.5 kDa (Figure 5a, purple bars) was directly compared to biosensor-determined relative As(III) uptake rate inhibition (red circles) to test the hypothesis that "free" As(III) smaller than 0.1-0.5 kDa describes the As fraction that can be taken up through microbial GlpF channels. Both measurements increased with greater Fe(III)/C ratios, and the >0.1-0.5 kDa size fraction provided the closest agreement with biosensor-determined uptake estimates. However, the extent of cellular uptake inhibition tended to be greater than the fraction of As(III) > 0.1–0.5 kDa, especially at low Fe(III)/C ratios. For AHA only, the fraction of As(III) > 0.1-0.5 kDa explained just 35.2 \pm 30.6% of the uptake inhibition observed for biosensor cells. This fraction steadily increased with greater Fe(III)/C ratios, until at the 900 μ g Fe/mg C ratio, the As(III) retention ratio >0.1-0.5 kDa was $86.2 \pm 27.6\%$ of the uptake inhibition and was not statistically different. Together, these results suggest that while As(III) binding to primarily colloidal particles explains a large fraction of inhibited cellular uptake at high Fe(III)/C ratios, at low Fe(III)/C ratios, there may be other processes regulating As(III) uptake.

Modeling of the pore radii of transport channels showed that the pore radii of the aquaglyceroporin channel GlpF that mediates uptake of glycerol and As(III) range from 0.1 to 0.3 kDa (Figure 5b). This indicates that As in size fractions >0.1—0.5 kDa would be excluded from uptake through GlpF due to size. Notably, the Lsi1 channel that mediates uptake of both orthosilicate and As(III) into rice⁶¹ has similar radii as GlpF, suggesting that inhibition of As(III) uptake into biosensor cells due to the molecular size of As(III)-bearing complexes or colloids may also be observed for uptake through Lsi1.

DISCUSSION

Oxic-anoxic interfaces in DOM-rich subsurface environments lead to formation of DOM-Fe(III) complexes and/or colloidal Fe(III) oxides that interact with As. 17,18,62 Our modeling results show that the effects of DOM and complexed and colloidal Fe(III) on As(III) bioavailability can be described well as a function of aqueous Fe(III) and DOC concentrations. The finding that DOM inhibited As(III) uptake into cells, particularly at low As(III)/C ratios (Figure 3 and Figure S7), is consistent with previous work from our laboratory using an aerobic biosensor assay to show that MNOM inhibited microbial As(III) uptake. Prior biosensor-based research has also shown that particulate (>0.22 μ m) Fe(III) oxides inhibit the cellular uptake of As(III), 63,64 but the current contribution is the first to our knowledge to probe effects of colloidal Fe using biosensor methods. Notably, cellular As(III) uptake was completely inhibited at an As(III)/C of 0.02 μ g

As/mg C when Fe(III)/C ratios >90 μ g Fe/mg C (Figure 3). This result shows that As(III) passing through a 0.22 μ m filter may have negligible bioavailability, a fact that is overlooked by the common assumption that "dissolved" As passing through a 0.22 μ m filter will be available.

It is well established that As(III) binds to Fe(III)-DOM complexes and/or colloidal Fe(III) oxides that are stabilized by DOM. 10,18,65 This work directly links these earlier measurements of the As(III) size fractionation to a direct measure of cellular uptake. This work also leverages the anaerobic biosensor approach to show that Fe(II) had a negligible effect on As(III) bioavailability (Figure S9). Results in Liao et al. 17 with AHA at molar Fe(II)/C ratios of 0.04 to 0.2 (equivalent to ~190 to ~900 μ g Fe(II)/mg C, within the range of the Fe(II)/C ratios used here) showed that 20–60% of Fe(II) was in the "small colloid" size fraction of $\sim 1-2$ to 20 nm. In our study, Fe(II) in this same range of Fe(II)/C ratios had no measurable effect on As(III) bioavailability. The effects of divalent and trivalent cations in cation bridging between As and DOM, and implications for As mobility and fate, have been studied for some time. 13,66 Catrouillet et al. 67 suggested that Fe(II) facilitated ternary complexation (or cation bridging) between DOM and As(III), but here, we provide novel experimental evidence that As(III) in any such complex must be weakly bound since there was no impact of Fe(II) on microbial uptake. The impact of Fe(III) but not Fe(II) on As(III) uptake underscores the importance of oxic-anoxic interfaces and the production of Fe(III) as a control on As(III) bioavailability.

There has been a further need to understand the effects of S_{Org} functional groups on binding of As(III) to organic matter 28,32,34,68 and resulting impacts on environmental As fate. Our results show that the S_{Org} content of DOM can be a good predictor of the inhibiting effects of DOM on As(III) bioavailability at low As(III)/C ratios and when Fe concentrations are low (Figure 4a and Figure S10), presumably due to the role of thiols as ligands for As(III) complexation. This finding is consistent with S_{Org}-dependent patterns in As(III)-DOM complexation reported by Abu-Ali et al.²⁶ and Hoffmann et al.²⁸ EXAFS results (Figure 4b) indicated that the mechanism for direct bonding between As(III) and AHA at low As(III)/C ratios is with S_{Org} ligands like thiols. This suggests that DOM with a higher S_{Org} content like MNOM can be more effective at binding As(III) and decreasing its availability to biota, but only if the reactive S_{Org} ligands are not saturated. In this analysis, we employed $S_{\rm Org}$ as a proxy for thiol densities due to challenges associated with direct thiol measurements, but we acknowledge that direct quantification of thiols, or of the reduced S_{org} fraction $(S_{Org, Red})$ that includes thiols, would likely provide better predictions of uptake inhibition. The S_{Org,Red} fraction of DOM can vary from ~20 to $\sim 80\%$. SRHA has been determined to have an $S_{\rm Org,Red}$ fraction of 64% of total S_{Org} using sulfur XANES, 69 and for AHA, the $S_{Org,Red}$ fraction has been determined to be in the range of 70-80% using XPS. The relatively high uptake inhibition in the presence of MNOM (Figure 4a) could be explained by its high thiol/S $_{\rm Org}$ ratio, estimated to be ${\sim}30\%$ in a previous report from our group. 43 The fact that uptake inhibition by AHA fell below the trendline could be due to thiols representing a small fraction of S_{Org,Red} in AHA or to impurities in AHA, which could occupy thiol sites. Notably, the copper (Cu) concentration of AHA was high (Table S1), and because Cu can also complex thiol ligands, 72,73 it is

possible that Cu impurities may have decreased complexation with As. Taken together, biosensor and EXAFS analyses clarify that the $S_{\rm Org}$ content (as a proxy for thiol ligand density) of DOM can be an important factor regulating the speciation and bioavailability of As but only at low As(III)/C ratios and low Fe(III) concentrations.

We hypothesized that the fraction of As(III) < 0.1-0.5 kDapore size would be the best predictor of bioavailability, since the aquaporin channel GlpF has pore radii between 0.1 and 0.3 kDa (Figure 5b), which excludes larger complexes or colloids. Results were partially consistent with this hypothesis, with the percentage of As(III) in size fractions >0.1-0.5 kDa providing the closest agreement with cellular uptake inhibition (Figure 5a). However, at low Fe(III)/C ratios, the biosensordetermined uptake inhibition systematically overestimated the amount of inhibition that would be expected based on the size fractionation of As(III) alone. These results suggest that at low Fe(III)/C ratios, there may be an additional mechanism beyond size exclusion that limits As(III) bioavailability. Prior work from our group with MNOM suggested that carbon catabolite repression could play a role in limiting As(III) uptake, 43 but this mechanism most likely does not play a role with AHA since biosensor growth curves were not significantly different in the presence of AHA compared to the control without AHA, indicating a lack of biolabile C (Figure S5). The different time scales of the biosensor and dialysis experiments (5 h vs 96 h, respectively) could have contributed to the discrepancy between As size fraction and uptake inhibition data. There was evidence for colloid aggregation over the longer time scale of the dialysis experiments, and changes in the colloidal properties may have affected As(III) binding. Biosensor and dialysis experiments were also performed at different temperatures, which could have led to differences in binding.

CONCLUSIONS

This research showed that the fraction of As(III) passing through a 0.22 μ m filter may be a poor proxy for As(III) bioavailability, with waters rich in both DOM and Fe(III) likely to have a larger fraction of As(III) in colloidal, nonbioavailable forms. The use of a recently developed anaerobic biosensor method revealed that complexed or colloidal Fe(III), and not Fe(II), strongly inhibited cellular uptake. These findings underscore the importance of oxicanoxic interfaces in DOM-rich subsurface environments in producing conditions where As(III) will be distributed in colloidal and nonbioavailable size fractions greater than 0.1-0.5 kDa but smaller than 0.22 μ m. Our results further showed that S_{Org}-rich DOM can play an important role in decreasing As(III) availability via complexation with S ligands but clarify that this role is probably limited to systems with low As(III)/C ratios and where concentrations of complexed/colloidal Fe(III) are low. Biosensor data provide a direct measurement of As(III) uptake into microbial cells, with direct relevance for microbial As transformations like methylation reactions that influence As speciation in rice grains^{4,77} and As volatilization from soils.⁵³ While biosensor data do not provide direct evidence of As(III) bioavailability for uptake into plants such as rice, the GlpF and Lsi1 channels that mediate As(III) transport into microbial and plant cells, respectively, have similar pore radii (Figure 4b), suggesting that factors related to molecular size that inhibit bioavailability would likely hold for both microbial and plant uptake.

ASSOCIATED CONTENT

5 Supporting Information

The Supporting Information is available free of charge at https://pubs.acs.org/doi/10.1021/acsestwater.3c00432.

Information on growth and exposure media, constitutive biosensor assay, and effects of other DOM properties on As uptake (PDF)

AUTHOR INFORMATION

Corresponding Author

Matthew C. Reid — School of Civil and Environmental Engineering, Cornell University, Ithaca, New York 14853, United States; orcid.org/0000-0001-5185-7678; Email: mcr239@cornell.edu

Authors

Hyun Yoon — School of Civil and Environmental Engineering, Cornell University, Ithaca, New York 14853, United States Benjamin Stenzler — Department of Biology, University of Ottawa, Ottawa K1N 6N5, Canada

Lena Abu-Ali – School of Civil and Environmental Engineering, Cornell University, Ithaca, New York 14853, United States

Maria P. Asta — Department of Mineralogy and Petrology, University of Granada, Granada 18071, Spain; orcid.org/0000-0001-6502-6744

Alexandre J. Poulain – Department of Biology, University of Ottawa, Ottawa K1N 6N5, Canada; orcid.org/0000-0002-0488-3993

Complete contact information is available at: https://pubs.acs.org/10.1021/acsestwater.3c00432

Author Contributions

CRediT: Hyun Yoon conceptualization, formal analysis, investigation, methodology, validation, visualization, writing-original draft; Benjamin Stenzler formal analysis, methodology, writing-review & editing; Maria P. Asta formal analysis; Lena Abu-Ali investigation; Alexandre J. Poulain conceptualization, funding acquisition, methodology, project administration, resources, supervision, writing-review & editing; Matthew C. Reid conceptualization, funding acquisition, project administration, resources, supervision, writing-review & editing.

Funding

Funding was provided by the NSF Environmental Chemical Sciences program award number 1905175 to M.C.R., USDA/NIFA grant number 2018-67019-27796 to M.C.R., and by the NSERC discovery grant program to A.J.P.

Notes

The authors declare no competing financial interest.

ACKNOWLEDGMENTS

The authors thank the anonymous reviewers whose careful comments helped to improve the quality of this manuscript. This research used resources of the National Synchrotron Light Source II, a U.S. Department of Energy (DOE) Office of Science User Facility operated for the DOE Office of Science by Brookhaven National Laboratory under Contract No. DE-SC0012704. The authors thank B. Ravel for assistance with beamtime at NSLS II.

REFERENCES

- (1) Wang, J.; Kerl, C. F.; Hu, P.; Martin, M.; Mu, T.; Brüggenwirth, L.; Wu, G.; Said-Pullicino, D.; Romani, M.; Wu, L.; Planer-Friedrich, B. Thiolated arsenic species observed in rice paddy pore waters. *Nat. Geosci.* 2020, 282–286.
- (2) Jia, Y.; Huang, H.; Zhong, M.; Wang, F.-H.; Zhang, L.-M.; Zhu, Y.-G. Microbial arsenic methylation in soil and rice rhizosphere. *Environ. Sci. Technol.* **2013**, 47 (7), 3141–3148.
- (3) Limmer, M. A.; Mann, J.; Amaral, D. C.; Vargas, R.; Seyfferth, A. L. Silicon-rich amendments in rice paddies: Effects on arsenic uptake and biogeochemistry. *Sci. Total Environ.* **2018**, *624*, 1360–1368.
- (4) Reid, M. C.; Maillard, J.; Bagnoud, A.; Falquet, L.; Le Vo, P.; Bernier-Latmani, R. Arsenic methylation dynamics in a rice paddy soil anaerobic enrichment culture. *Environ. Sci. Technol.* **2017**, *51* (18), 10546–10554.
- (5) Masscheleyn, P. H.; Delaune, R. D.; Patrick, W. H., Jr. Effect of redox potential and pH on arsenic speciation and solubility in a contaminated soil. *Environ. Sci. Technol.* **1991**, 25 (8), 1414–1419.
- (6) Saunders, J.; Lee, M.-K.; Shamsudduha, M.; Dhakal, P.; Uddin, A.; Chowdury, M.; Ahmed, K. Geochemistry and mineralogy of arsenic in (natural) anaerobic groundwaters. *Appl. Geochem.* **2008**, 23 (11), 3205–3214.
- (7) Xu, L.; Wu, X.; Wang, S.; Yuan, Z.; Xiao, F.; Yang, M.; Jia, Y. Speciation change and redistribution of arsenic in soil under anaerobic microbial activities. *J. Hazardous Mater.* **2016**, *301*, 538–546.
- (8) Tufano, K. J.; Reyes, C.; Saltikov, C. W.; Fendorf, S. Reductive processes controlling arsenic retention: revealing the relative importance of iron and arsenic reduction. *Environ. Sci. Technol.* **2008**, 42 (22), 8283–8289.
- (9) Bauer, M.; Blodau, C. Arsenic distribution in the dissolved, colloidal and particulate size fraction of experimental solutions rich in dissolved organic matter and ferric iron. *Geochim. Cosmochim. Acta* **2009**, 73 (3), 529–542.
- (10) Liu, G.; Fernandez, A.; Cai, Y. Complexation of arsenite with humic acid in the presence of ferric iron. *Environ. Sci. Technol.* **2011**, 45 (8), 3210–3216.
- (11) Zhang, H.; Selim, H. Colloid mobilization and arsenite transport in soil columns: Effect of ionic strength. *J. Environ. Qual.* **2007**, *36* (5), 1273–1280.
- (12) Buschmann, J.; Kappeler, A.; Lindauer, U.; Kistler, D.; Berg, M.; Sigg, L. arsenite and arsenate binding to dissolved humic acids: influence of pH, type of humic acid, and aluminum. *Environ. Sci. Technol.* **2006**, *40* (19), 6015–6020.
- (13) Sharma, P.; Ofner, J.; Kappler, A. Formation of binary and ternary colloids and dissolved complexes of organic matter, Fe and As. *Environ. Sci. Technol.* **2010**, 44 (12), 4479–4485.
- (14) Sundman, A.; Karlsson, T.; Sjöberg, S.; Persson, P. Complexation and precipitation reactions in the ternary As(V)–Fe(III)–OM (organic matter) system. *Geochim. Cosmochim. Acta* **2014**, *145*, 297–314.
- (15) ThomasArrigo, L. K.; Mikutta, C.; Byrne, J.; Barmettler, K.; Kappler, A.; Kretzschmar, R. Iron and arsenic speciation and distribution in organic flocs from streambeds of an arsenic-enriched peatland. *Environ. Sci. Technol.* **2014**, 48 (22), 13218–13228.
- (16) Hong, Z.; Hu, S.; Yang, Y.; Deng, Z.; Li, X.; Liu, T.; Li, F. The key roles of Fe oxyhydroxides and humic substances during the transformation of exogenous arsenic in a redox-alternating acidic paddy soil. *Water Res.* 2023, No. 120286.
- (17) Liao, P.; Li, W.; Jiang, Y.; Wu, J.; Yuan, S.; Fortner, J. D.; Giammar, D. E. Formation, aggregation, and deposition dynamics of NOM-iron colloids at anoxic—oxic interfaces. *Environ. Sci. Technol.* **2017**, *51* (21), 12235–12245.
- (18) Ritter, K.; Aiken, G. R.; Ranville, J. F.; Bauer, M.; Macalady, D. L. Evidence for the aquatic binding of arsenate by natural organic matter—suspended Fe(III). *Environ. Sci. Technol.* **2006**, *40* (17), 5380–5387.
- (19) Brune, A.; Frenzel, P.; Cypionka, H. Life at the oxic-anoxic interface: microbial activities and adaptations. *FEMS Microbiol. Rev.* **2000**, 24 (5), 691–710.

- (20) Amaral, D. C.; Lopes, G.; Guilherme, L. R.; Seyfferth, A. L. A new approach to sampling intact Fe plaque reveals Si-induced changes in Fe mineral composition and shoot As in rice. *Environ. Sci. Technol.* **2017**, *51* (1), 38–45.
- (21) Hansel, C. M.; Fendorf, S.; Sutton, S.; Newville, M. Characterization of Fe plaque and associated metals on the roots of mine-waste impacted aquatic plants. *Environ. Sci. Technol.* **2001**, 35 (19), 3863–3868.
- (22) Maguffin, S. C.; Abu-Ali, L.; Tappero, R. V.; Pena, J.; Rohila, J. S.; McClung, A. M.; Reid, M. C. Influence of manganese abundances on iron and arsenic solubility in rice paddy soils. *Geochim. Cosmochim. Acta* **2020**, *276*, 50–69.
- (23) Abu-Ali, L.; Maguffin, S. C.; Rohila, J. S.; McClung, A. M.; Reid, M. C. Effects of alternate wetting and drying on oxyanion-forming and cationic trace elements in rice paddy soils: impacts on arsenic, cadmium, and micronutrients in rice. *Environ. Geochem. Health* 2023, 1–17.
- (24) Guénet, H.; Davranche, M.; Vantelon, D.; Bouhnik-Le Coz, M.; Jardé, E.; Dorcet, V.; Demangeat, E.; Jestin, J. Highlighting the wide variability in arsenic speciation in wetlands: A new insight into the control of the behavior of arsenic. *Geochim. Cosmochim. Acta* 2017, 203, 284–302.
- (25) Gontijo, E. S.; Watanabe, C. H.; Monteiro, A. S.; Tonello, P. S.; da Silva, G. A.; Friese, K.; Roeser, H. M.; Rosa, A. H. Distribution and bioavailability of arsenic in natural waters of a mining area studied by ultrafiltration and diffusive gradients in thin films. *Chemosphere* **2016**, 164, 290–298.
- (26) Abu-Ali, L.; Yoon, H.; Reid, M. C. Effects of organic sulfur and arsenite/dissolved organic matter ratios on arsenite complexation with dissolved organic matter. *Chemosphere* **2022**, *302*, No. 134770.
- (27) Pothier, M. P.; Lenoble, V.; Garnier, C.; Misson, B.; Rentmeister, C.; Poulain, A. J. Dissolved organic matter controls of arsenic bioavailability to bacteria. *Sci. Total Environ.* **2020**, *716*, No. 137118.
- (28) Hoffmann, M.; Mikutta, C.; Kretzschmar, R. Bisulfide reaction with natural organic matter enhances arsenite sorption: insights from X-ray absorption spectroscopy. *Environ. Sci. Technol.* **2012**, *46* (21), 11788–11797.
- (29) Spuches, A. M.; Kruszyna, H. G.; Rich, A. M.; Wilcox, D. E. Thermodynamics of the As(III)— thiol interaction: arsenite and monomethylarsenite complexes with glutathione, dihydrolipoic acid, and other thiol ligands. *Inorg. Chem.* **2005**, *44* (8), 2964–2972.
- (30) Langner, P.; Mikutta, C.; Kretzschmar, R. Arsenic sequestration by organic sulphur in peat. *Nat. Geosci.* **2012**, *5* (1), 66–73.
- (31) Catrouillet, C.; Davranche, M.; Dia, A.; Bouhnik-Le Coz, M.; Pédrot, M.; Marsac, R.; Gruau, G. Thiol groups controls on arsenite binding by organic matter: New experimental and modeling evidence. *J. Colloid Interface Sci.* **2015**, *460*, 310–320.
- (32) Eberle, A.; Besold, J.; Kerl, C. F.; Lezama Pacheco, J.; Fendorf, S.; Planer-Friedrich, B. Arsenic fate in peat controlled by pH-dependent role of reduced sulfur. *Environ. Sci. Technol.* **2020**, 54 (11), 6682–6692.
- (33) Besold, J.; Biswas, A.; Suess, E.; Scheinost, A. C.; Rossberg, A.; Mikutta, C.; Kretzschmar, R.; Gustafsson, J. P.; Planer-Friedrich, B. Monothioarsenate transformation kinetics determining arsenic sequestration by sulfhydryl groups of peat. *Environ. Sci. Technol.* **2018**, *52* (13), 7317–7326.
- (34) Biswas, A.; Besold, J.; Sjöstedt, C.; Gustafsson, J. P.; Scheinost, A. C.; Planer-Friedrich, B. Complexation of arsenite, arsenate, and monothioarsenate with oxygen-containing functional groups of natural organic matter: an XAS study. *Environ. Sci. Technol.* **2019**, 53 (18), 10723–10731.
- (35) Tran, H. T.; Vu, N. D.; Matsukawa, M.; Okajima, M.; Kaneko, T.; Ohki, K.; Yoshikawa, S. Heavy metal biosorption from aqueous solutions by algae inhabiting rice paddies in Vietnam. *J. Environ. chemical Eng.* **2016**, 4 (2), 2529–2535.
- (36) Tang, Y.; Zhang, M.; Sun, G.; Pan, G. Impact of eutrophication on arsenic cycling in freshwaters. *Water Res.* **2019**, *150*, 191–199.

- (37) Wang, J.; Bai, L.; Zeng, X.; Su, S.; Wang, Y.; Wu, C. Assessment of arsenic availability in soils using the diffusive gradients in thin films (DGT) technique—a comparison study of DGT and classic extraction methods. *Environ. Sci.: Process. Impacts* **2014**, *16* (10), 2355–2361.
- (38) Hinz, A. J.; Stenzler, B.; Poulain, A. J.; Bose, A. Golden gate assembly of aerobic and anaerobic microbial bioreporters. *Appl. Environ. Microbiol.* **2022**, 88 (1), No. e01485-21.
- (39) Saitoh, Y.; Mitani-Ueno, N.; Saito, K.; Matsuki, K.; Huang, S.; Yang, L.; Yamaji, N.; Ishikita, H.; Shen, J. R.; Ma, J. F.; Suga, M. Structural basis for high selectivity of a rice silicon channel Lsi1. *Nat. Commun.* **2021**, *12* (1), 6236.
- (40) Fu, D.; Libson, A.; Miercke, L. J.; Weitzman, C.; Nollert, P.; Krucinski, J.; Stroud, R. M. Structure of a glycerol-conducting channel and the basis for its selectivity. *Science* **2000**, 290 (5491), 481–486.
- (41) Pan, C.; Troyer, L. D.; Liao, P.; Catalano, J. G.; Li, W.; Giammar, D. E. Effect of humic acid on the removal of chromium(VI) and the production of solids in iron electrocoagulation. *Environ. Sci. Technol.* **2017**, *51* (11), 6308–6318.
- (42) Hering, J. G.; Morel, F. M. Humic acid complexation of calcium and copper. *Environ. Sci. Technol.* **1988**, 22 (10), 1234–1237.
- (43) Yoon, H.; Giometto, A.; Pothier, M. P.; Zhang, X.; Poulain, A. J.; Reid, M. C.; Glass, J. B. Time-dependent biosensor fluorescence as a measure of bacterial arsenic uptake kinetics and its inhibition by dissolved organic matter. *Appl. Environ. Microbiol.* **2022**, 88 (16), No. e00891-22.
- (44) Neidhardt, F. C. Escherichia coli and Salmonella: cellular and molecular biology. *Science* **1996**, 1678.
- (45) Tajkhorshid, E.; Nollert, P.; Jensen, M. Ø.; Miercke, L. J.; O'Connell, J.; Stroud, R. M.; Schulten, K. Control of the selectivity of the aquaporin water channel family by global orientational tuning. *Science* **2002**, *296* (5567), 525–530.
- (46) Sehnal, D.; Svobodová Vařeková, R.; Berka, K.; Pravda, L.; Navrátilová, V.; Banáš, P.; Ionescu, C. M.; Otyepka, M.; Koča, J. MOLE 2.0: advanced approach for analysis of biomacromolecular channels. *J. Cheminform.* **2013**, *5*, 1–13.
- (47) Pettersen, E. F.; Goddard, T. D.; Huang, C. C.; Couch, G. S.; Greenblatt, D. M.; Meng, E. C.; Ferrin, T. E. UCSF Chimera—a visualization system for exploratory research and analysis. *J. Comput. Chem.* **2004**, 25 (13), 1605–1612.
- (48) Scott, N.; Hatlelid, K. M.; MacKenzie, N. E.; Carter, D. E. Reactions of arsenic(III) and arsenic(V) species with glutathione. *Chemical research in toxicology* **1993**, *6* (1), 102–106.
- (49) Smith, P. G.; Koch, I.; Gordon, R. A.; Mandoli, D. F.; Chapman, B. D.; Reimer, K. J. X-ray absorption near-edge structure analysis of arsenic species for application to biological environmental samples. *Environ. Sci. Technol.* **2005**, 39 (1), 248–254.
- (50) George, G. N.; Pickering, I. J. EXAFSPAK: A suite of computer programs for analysis of X-ray absorption spectra. Stanford Synchrotron Radiation Laboratory: Stanford, CA, USA, 1995.
- (51) Rehr, J. J.; Kas, J. J.; Vila, F. D.; Prange, M. P.; Jorissen, K. Parameter-free calculations of X-ray spectra with FEFF9. *Phys. Chem. Chem. Phys.* **2010**, *12* (21), 5503–5513.
- (52) Ravel, B. ATOMS: crystallography for the X-ray absorption spectroscopist. *Journal of synchrotron radiation* **2001**, 8 (2), 314–316.
- (53) Zhang, X.; Reid, M. C. Inhibition of methanogenesis leads to accumulation of methylated arsenic species and enhances arsenic volatilization from rice paddy soil. *Science of The Total Environment* **2022**, *818*, No. 151696.
- (54) Viollier, E.; Inglett, P.; Hunter, K.; Roychoudhury, A.; Van Cappellen, P. The ferrozine method revisited: Fe(II)/Fe(III) determination in natural waters. *Applied geochemistry* **2000**, *15* (6), 785–790.
- (55) Bone, S. E.; Bargar, J. R.; Sposito, G. Mackinawite (FeS) reduces mercury(II) under sulfidic conditions. *Environ. Sci. Technol.* **2014**, *48* (18), 10681–10689.
- (56) Chriswell, C. D.; Mroch, D. R.; Markuszewski, R. Determination of total sulfur by ion chromatography following

- peroxide oxidation in spent caustic from the chemical cleaning of coal. *Anal. Chem.* **1986**, *58* (2), 319–321.
- (57) Helms, J. R.; Stubbins, A.; Ritchie, J. D.; Minor, E. C.; Kieber, D. J.; Mopper, K. Absorption spectral slopes and slope ratios as indicators of molecular weight, source, and photobleaching of chromophoric dissolved organic matter. *Limnology and oceanography* **2008**, 53 (3), 955–969.
- (58) Weishaar, J. L.; Aiken, G. R.; Bergamaschi, B. A.; Fram, M. S.; Fujii, R.; Mopper, K. Evaluation of specific ultraviolet absorbance as an indicator of the chemical composition and reactivity of dissolved organic carbon. *Environ. Sci. Technol.* **2003**, *37* (20), 4702–4708.
- (59) RStudio, T. RStudio: integrated development for R. Rstudio Team, PBC: Boston, MA, URL http://www.rstudio.com 2020.
- (60) Skyllberg, U.; Qian, J.; Frech, W. Combined XANES and EXAFS study on the bonding of methyl mercury to thiol groups in soil and aquatic organic matter. *Phys. Scr.* **2005**, 2005 (T115), 894.
- (61) Ma, J. F.; Yamaji, N.; Mitani, N.; Xu, X.-Y.; Su, Y.-H.; McGrath, S. P.; Zhao, F.-J. Transporters of arsenite in rice and their role in arsenic accumulation in rice grain. *Proc. Natl. Acad. Sci. U. S. A.* **2008**, 105 (29), 9931–9935.
- (62) Bauer, M.; Blodau, C. Mobilization of arsenic by dissolved organic matter from iron oxides, soils and sediments. *Sci. Total Environ.* **2006**, 354 (2–3), 179–190.
- (63) Harms, H.; Rime, J.; Leupin, O.; Hug, S. J.; van der Meer, J. R. Effect of groundwater composition on arsenic detection by bacterial biosensors. *Microchimica Acta* **2005**, *151*, 217–222.
- (64) van Genuchten, C. M.; Finger, A.; van der Meer, J. R.; Peña, J. Bacterial bioreporter detection of arsenic associated with iron oxides. *Environmental Science: Processes & Impacts* **2018**, 20 (6), 913–922.
- (65) Liu, G.; Cai, Y. Studying arsenite—humic acid complexation using size exclusion chromatography—inductively coupled plasma mass spectrometry. *Journal of hazardous materials* **2013**, 262, 1223—1229.
- (66) Sharma, P.; Rolle, M.; Kocar, B.; Fendorf, S.; Kappler, A. Influence of natural organic matter on As transport and retention. *Environ. Sci. Technol.* **2011**, 45 (2), 546–553.
- (67) Catrouillet, C.; Davranche, M.; Dia, A.; Bouhnik-Le Coz, M.; Demangeat, E.; Gruau, G. Does As(III) interact with Fe(II), Fe(III) and organic matter through ternary complexes? *J. Colloid Interface Sci.* **2016**, *470*, 153–161.
- (68) Lenoble, V.; Dang, D. H.; Loustau Cazalet, M.; Mounier, S.; Pfeifer, H. R.; Garnier, C. Evaluation and modelling of dissolved organic matter reactivity toward As(III) and As(V)–Implication in environmental arsenic speciation. *Talanta* **2015**, *134*, 530–537.
- (69) Manceau, A.; Nagy, K. L. Quantitative analysis of sulfur functional groups in natural organic matter by XANES spectroscopy. *Geochim. Cosmochim. Acta* **2012**, *99*, 206–223.
- (70) Urban, N.; Ernst, K.; Bernasconi, S. Addition of sulfur to organic matter during early diagenesis of lake sediments. *Geochimica et cosmochimica acta* **1999**, *63* (6), 837–853.
- (71) Sachs, S.; Reich, T.; Bernhard, G. Study of the role of sulfur functionalities in humic acids for uranium(VI) complexation. *Radiochim. Acta* **2010**, *98* (8), 467–477.
- (72) Laglera, L. M.; van den Berg, C. M. Copper complexation by thiol compounds in estuarine waters. *Marine Chemistry* **2003**, *82* (1–2), 71–89.
- (73) Nogueira, P.; Melão, M.; Lombardi, A.; Nogueira, M. Natural DOM affects copper speciation and bioavailability to bacteria and ciliate. *Archives of environmental contamination and toxicology* **2009**, *57*, 274–281.
- (74) Egli, T. How to live at very low substrate concentration. *Water Res.* **2010**, *44* (17), 4826–4837.
- (75) Chen, S.; Oldham, M. L.; Davidson, A. L.; Chen, J. Carbon catabolite repression of the maltose transporter revealed by X-ray crystallography. *Nature* **2013**, *499* (7458), 364–368.
- (76) Görke, B.; Stülke, J. Carbon catabolite repression in bacteria: many ways to make the most out of nutrients. *Nature Reviews Microbiology* **2008**, *6* (8), 613–624.

(77) Chen, C.; Li, L.; Huang, K.; Zhang, J.; Xie, W.-Y.; Lu, Y.; Dong, X.; Zhao, F.-J. Sulfate-reducing bacteria and methanogens are involved in arsenic methylation and demethylation in paddy soils. *ISME Journal* **2019**, *13* (10), 2523–2535.